

# DAIS: Automatic Channel Pruning via Differentiable Annealing Indicator Search

Yushuo Guan<sup>1</sup>, Ning Liu<sup>2</sup>, Pengyu Zhao<sup>1</sup>, Zhengping Che<sup>2</sup>, Kaigui Bian<sup>1</sup>, Yanzhi Wang<sup>3</sup>, Jian Tang<sup>2</sup>

<sup>1</sup>Peking University, <sup>2</sup>Didi Chuxing, <sup>3</sup>Northeastern University

david.guan@pku.edu.cn, neilliuning@didiglobal.com, pengyuzhao@pku.edu.cn, chezhengping@didiglobal.com, bkg@pku.edu.cn, yanz.wang@northeastern.edu, tangjian@didiglobal.com

## Abstract

The convolutional neural network has achieved great success in fulfilling computer vision tasks despite large computation overhead against efficient deployment. Structured (channel) pruning is usually applied to reduce the model redundancy while preserving the network structure, such that the pruned network can be easily deployed in practice. However, existing structured pruning methods require hand-crafted rules which may lead to tremendous pruning space. In this paper, we introduce Differentiable Annealing Indicator Search (DAIS) that leverages the strength of neural architecture search in the channel pruning and automatically searches for the effective pruned model with given constraints on computation overhead. Specifically, DAIS relaxes the binarized channel indicators to be continuous and then jointly learns both indicators and model parameters via bi-level optimization. To bridge the non-negligible discrepancy between the continuous model and the target binarized model, DAIS proposes an annealing-based procedure to steer the indicator convergence towards binarized states. Moreover, DAIS designs various regularizations based on *a priori* structural knowledge to control the pruning sparsity and to improve model performance. Experimental results show that DAIS outperforms state-of-the-art pruning methods on CIFAR-10, CIFAR-100, and ImageNet.

## 1 Introduction

In recent years, the community has achieved great success on various computer vision tasks (Goodfellow et al. 2014; Taigman et al. 2014; Newell, Yang, and Deng 2016; He et al. 2017) by designing deeper and wider convolutional neural networks (CNNs). Despite the superior performance of these networks, the computation cost is burdensome. Hence, it is difficult to directly deploy such “expensive” networks over computation-limited platforms such as robotics, self-driving vehicles, and most of the mobile devices. A straightforward solution to tackle the problem is *channel pruning*, which reduces the computation cost of the network by eliminating redundant channels. It requires no extra hardware support and is perfectly compatible with representative deep learning acceleration frameworks, such as TVM (Chen et al. 2018), TFLite (Ten 2017), and Alibaba MNN (Jiang et al. 2020).

Earlier channel pruning methods leverage hand-crafted criteria, such as lasso regression (Liu et al. 2017) and geometric median-based criterion (He et al. 2019), to filter

out unimportant channels. Recent research on pruning (Liu et al. 2018) implies that the pruning process is equivalent to searching a compact network structure, suggesting the possibility of automatic channel pruning. Since the pruning search space increases exponentially with original networks being deeper and wider, a potential approach to address this problem is through the idea of neural architecture search (NAS) with less human interaction and expert effort. Standard NAS focuses on the network topology optimization and is typically performed prior to pruning with a much higher search cost. To break the limitation, AMC (He et al. 2018b) searches for important channels automatically by reinforcement learning. However, it only prunes the middle channels of the blocks with shortcut (like ResNet), which limits the optimal upper bound of the pruning ratio. TAS (Dong and Yang 2019) trains a supernet in the channel search process and derives a pruned model from the supernet, but the architecture discrepancies between the supernet and the pruned model may lead to degraded performance in terms of both pruning ratio and accuracy.

To address these problems in the automatic pruning approaches, we propose DAIS, a Differentiable Annealing Indicator Search method for channel pruning, taking advantage of differentiable neural architecture search (Liu, Simonyan, and Yang 2019). In general, DAIS first searches for a pruned model in an automatic manner with computational constraints and then fine-tunes the derived model. Specifically, DAIS introduces binarized channel indicators and utilizes continuous auxiliary parameters to relax the indicators for optimization. Then it jointly learns model parameters and auxiliary parameters via bi-level optimization, to simultaneously obtain the accurate model and identify the importance of each channel. An annealing-relaxed function is incorporated into the channel indicators to mitigate the discrepancy between the derived pruned model and the pre-trained supernet for the search procedure. The indicators are initialized to be gently continuous at high temperatures, and gradually converge to binarized states as the training proceeds and temperature anneals. Furthermore, to provide the structural constraints on the pruned model, we design dedicated regularizers in DAIS: 1) A continuous FLOPs estimator regularizer that controls the computational cost of the pruned model, and 2) a symmetry regularizer which optimizes the gradient propagation on the pruned ultra-deep

neural networks with residual connections. Additionally, compared with most existing methods requiring multi-round pruning, DAIS is a one-shot solution which is elegant and efficient. Experimental results show that DAIS outperforms state-of-the-art pruning methods on representative datasets such as CIFAR-10 (Krizhevsky, Hinton et al. 2009), CIFAR-100 (Krizhevsky, Hinton et al. 2009), and ImageNet (Deng et al. 2009).

The main contributions of this paper are as follows.

1) We propose DAIS, a differentiable annealing indicator search framework for channel pruning, which leverages the gradient-based bi-level optimization to search for appropriate pruned models with sparsity requirements. 2) We design an annealing-relaxed channel indicator function for the differentiable search process. This function is initialized to be continuous to relax the search process differentiable and then gradually converges into binarization to produce the pruned model. 3) We design different regularizers to constrain the computational cost of the pruned model. 4) DAIS achieves state-of-the-art performance on different datasets and models, and extensive experiments and ablation studies demonstrate its effectiveness.

## 2 Related Works

**Channel pruning.** The recent advances of network pruning mainly fall into two categories: unstructured pruning and structured (channel) pruning. Unstructured pruning removes weights at arbitrary locations, but the resulted sparse matrix and indexing scheme limit the practical acceleration. To avoid these limitations, recent works (Luo, Wu, and Lin 2017; He, Zhang, and Sun 2017; Yu et al. 2018; Zhuang et al. 2018; He et al. 2019; Liu et al. 2020) focus on channel(filter)-level pruning. The pruned model would maintain the network structure and take full advantages of Basic Linear Algebra Subprograms (BLAS) operations. Thus it can be perfectly supported by the prevalent CNN acceleration frameworks (Ten 2017; Chen et al. 2018; Jiang et al. 2020). Early work (Wen et al. 2016) heuristically evaluates the importance by the magnitude of the weights, which adopts group lasso to force groups of weights to be smaller and filter out the channels with zero weights. FPGM (He et al. 2019) filters out redundant channels with a criterion of the geometric median. Recently, CNN-FCF (Li et al. 2019) learns binary scalars associated with filters to determine the target filters to prune. The binary scalars are not differentiable, and additional optimization tools (such as ADMM) are needed for addressing the binary constraints.

**Neural architecture search (NAS).** Recently, there has been a growing interest in automatically designing neural network architecture. Prior works mainly sample a large number of networks from search space and train them from scratch to obtain a supervision signal, e.g., validation accuracy, for optimizing the sampling agent with reinforcement learning (Baker et al. 2017; Zoph and Le 2017; Zoph et al. 2018; Tan et al. 2019) or updating the population with the evolutionary algorithm (Real et al. 2017, 2019). Recent attempts (Bender et al. 2018; Pham et al. 2018; Chen et al. 2019; Li and Talwalkar 2019; Wu et al. 2019; Xie et al. 2019) introduce weight-sharing paradigm in NAS to boost

search efficiency, where all candidate sub-networks share the weights in a single one-shot model that contains every possible architecture in the search space. Among weight-sharing methods, DARTS (Liu, Simonyan, and Yang 2019) has attracted much attention. It relaxes the search space to be continuous with architecture parameters and then efficiently optimizes model parameters and architecture parameters together via gradient descent.

**Automatic channel pruning.** The idea of NAS has been leveraged to guide network pruning, resulting in typically less search cost than the complete NAS. NetSlimming (Liu et al. 2017) automatically selects filters by associating scaling factors from batch normalization (BN) layers and prunes filters with smaller scaling factors. AMC (He et al. 2018b) leverages deep reinforcement learning to determine the pruning rate of each layer. It uses a sampling, estimating, and learning process, which is time-consuming especially for deep networks. TAS (Dong and Yang 2019) directly searches the width and depth of a network with a novel transformable architecture search procedure, but there are architecture discrepancies between the supernet in the search procedure and the pruned model, which may result in degraded performance in terms of pruning ratio and accuracy.

## 3 Methodology

In this section, we firstly formulate the channel pruning task and then introduce the Differentiable Annealing Indicator Search (DAIS) method for channel pruning. Specifically, we demonstrate the differentiable channel indicator search procedure of DAIS, propose the annealing-relaxed channel indicator, and introduce three regularizers for structural restrictions. The overview of DAIS is illustrated in Figure 1.

### 3.1 Problem Definition

A general CNN model is built with a stack of convolutional layers. Suppose the model has  $L$  layers, and we define  $O_l$  as the output feature tensor of the  $l$ -th convolutional layer. The computation process of  $O_l$  can be commonly depicted as:

$$O_l = F_l(W_l, O_{l-1}), \quad (1)$$

where  $W_l \in \mathcal{R}^{k_l \times k_l \times c_{l-1} \times c_l}$  denotes the convolutional kernel of the  $l$ -th layer with input channel of  $c_{l-1}$  and output channel of  $c_l$ , and  $F_l(\cdot)$  represents the convolution function. The optimization target of model pruning is to derive the network architecture with the minimum number of convolutional filters from the original model while maintaining accuracy. The channel pruning further preserves the structural information of CNN and only reduces the number of channels, i.e.,  $c_l$  for each layer.

A popular channel pruning approach (Liu et al. 2017) introduces channel indicators, which are binarized vectors generating sparsity for each convolutional layer, i.e.:

$$O'_l = F_l(W_l, O'_{l-1}) \otimes I_l, \quad (2)$$

where  $I_l \in \{0, 1\}^{c_l}$  denotes the indicator vector,  $\otimes$  represents the tensor product, and  $O'_l$  denotes the masked

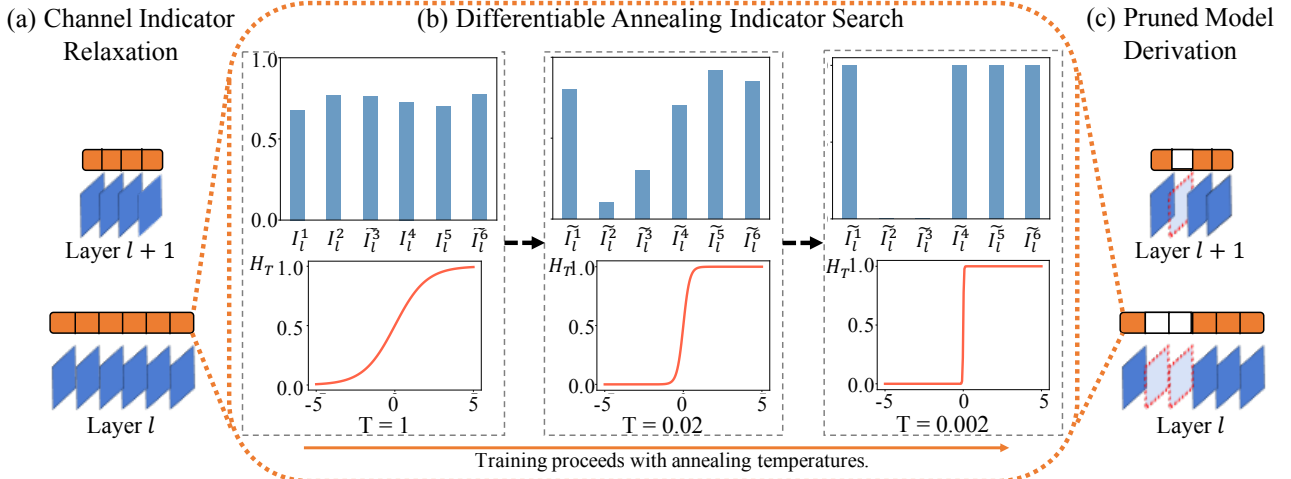


Figure 1: Overview of the Differentiable Annealing Indicator Search (DAIS) framework. (a) Channel indicator relaxation. We build annealing-relaxed channel indicators for each convolutional layer. (b) Differentiable annealing indicator search. As the training proceeds, the annealing-relaxed indicator  $\tilde{I}_l^i$  will converge to binarization with annealing temperatures, as illustrated in the histograms.  $h_T(*)$  is an annealing function, which approximates the binarized state when the temperature anneals. (c) Pruned model derivation. The output channels with  $\tilde{I}_l^i = 0$  are pruned from the original model.

(pruned) output tensor by  $I_l$ . With channel indicator, the optimization target of channel pruning can be represented by:

$$\min_{\mathcal{W}, \mathcal{I}} \mathcal{L}(\mathcal{W}, \mathcal{I}) + \lambda \mathcal{R}(\mathcal{I}), \quad (3)$$

where  $\mathcal{W} = [W_1, W_2, \dots, W_L]$  and  $\mathcal{I} = [I_1, I_2, \dots, I_L]$  denote respectively the parameter and indicator sets,  $\mathcal{L}(\cdot)$  denotes the loss function, and  $\mathcal{R}(\cdot)$  denotes the regularizer that induces the structural restrictions. The details of regularizers will be discussed in Sec. 3.4.

As the channel indicator is binarized and non-differentiable, it could not be learned directly by conventional gradient descent methods. Therefore, some channel pruning approaches (Liu et al. 2017; You et al. 2019) associate the channel indicator with differentiable metrics, e.g., leverage the weights in batch normalization (BN) as an indirect indicator, and zero out the channels with small BN weights (Liu et al. 2017). Instead of building up these indirect associations, we deal with the channel indicator from another perspective which is more effective and flexible, i.e., *relax the channel indicators to be continuous, and then jointly learn the model parameters and relaxed channel indicators via a differentiable search procedure.*

### 3.2 Differentiable Indicator Search

The differentiable search procedure is widely used in NAS (Chu et al. 2019; Liu, Simonyan, and Yang 2019; Wu et al. 2019) but seldom explored towards solving the channel pruning problem. In this section, we incorporate the idea of differentiable search into channel pruning and introduce the differentiable indicator search.

To make the search space continuous, we relax each binarized channel indicator  $I_l^i$ ,  $i \in [1, c_l]$ , into a relaxed channel indicator  $\tilde{I}_l^i$  parameterized by an auxiliary parameter  $\alpha_l^i$

(discussed in Sec. 3.3). After the relaxation, the goal of the indicator search is to jointly learn model parameters  $\mathcal{W}$  and auxiliary parameters  $\alpha$ . An intuitive option of optimization is to update  $\mathcal{W}$  and  $\alpha$  simultaneously on the training set, but the simultaneous optimization will cause  $\alpha$  to overfit on the training set, which might derive the pruned result with poor generalization. Therefore, we leverage the bi-level optimization in the differentiable indicator search procedure, with  $\alpha$  as the upper-level variable and  $\mathcal{W}$  as the lower-level variable. Specifically, it searches for  $\alpha^*$  that minimizes the combination of validation loss  $\mathcal{L}_{\text{val}}(\mathcal{W}^*(\alpha), \alpha)$  and regularizers  $\mathcal{R}(\alpha)$ , where the values of model parameters  $\mathcal{W}^*$  are obtained by minimizing the training loss  $\mathcal{L}_{\text{train}}(\mathcal{W}, \alpha)$ :

$$\min_{\alpha} \mathcal{L}_{\text{val}}(\mathcal{W}^*(\alpha), \alpha) + \lambda \mathcal{R}(\alpha), \quad (4)$$

$$\text{s.t. } \mathcal{W}^*(\alpha) = \arg \min_{\mathcal{W}} \mathcal{L}_{\text{train}}(\mathcal{W}, \alpha). \quad (5)$$

To solve the bi-level optimization problem,  $\mathcal{W}$  and  $\alpha$  are updated in a multi-step scheme by gradient descent on training and validation sets, and finally reach the local minima. The alternating gradient updating process resembles (Liu, Simonyan, and Yang 2019) with more details provided in the reference paper.

### 3.3 Annealing-Relaxed Channel Indicator

To make the relaxed channel indicator a better approximation of binarized channel indicator, the value range for each entry  $\tilde{I}_l^i$  should be limited between 0 and 1. Hence, a straightforward solution is to use a sigmoid function over auxiliary parameters, formally:

$$\tilde{I}_l^i = \frac{1}{1 + e^{-\alpha_l^i}}. \quad (6)$$

However, the above approximation has two inevitable problems. (1) The resulting  $\tilde{I}_l^i$  might not converge to sparse values, i.e., close to 0 or 1, as there is no guarantee for sparsity based on the continuous auxiliary parameters. Hence, a hand-crafted threshold is still required to binarize the final pruning result, which limits the robustness of this method and makes it against our motivation of automatic channel pruning. (2) Moreover, the discretization brings non-negligible discrepancy between the continuous search result and binarized model (Arber Zela et al. 2019; Chu et al. 2019; Liu, Simonyan, and Yang 2019). This could deteriorate the accuracy of the pruned model when joint parameters of  $W$  and  $\alpha$  stuck in sharp local minima where a small perturbation can lead to large performance degradation.

We propose an annealing-relaxed channel indicator to fill the discrepancy. Concretely, we add a temperature variable  $T$  on the sigmoid function, which is set to be high at the beginning and gradually anneals to zero at the end of training. As a result, the indicator is initially continuous to support the gradient update of the auxiliary parameters, and finally converges to the binarized state that leads to the pruned model:

$$\tilde{I}_l^i = H_T(\alpha_l^i) = \frac{1}{1 + e^{-\alpha_l^i/T}}, \quad I_l^i = \lim_{T \rightarrow 0} H_T(\alpha_l^i), \quad (7)$$

where  $\alpha_l^i$  represents the auxiliary parameter. The annealing-relaxed function  $H_T(\cdot)$  is initialized with a high temperature  $T = T_0$ . When the training proceeds into  $n$ -th epoch, the temperature of  $H_T$  anneals to  $T_0/\sigma(n)$ , where  $\sigma(\cdot)$  denotes the temperature annealing scheme. Finally, the discrete  $I_l^i$  can be approached with  $T \rightarrow 0$  at the end of the search.

### 3.4 Structural Restrictions by Regularizers

The vanilla cross-entropy loss itself is infeasible to induce *a priori* structural restrictions, e.g., the number of floating point operations (FLOPs), which play a critical role in pruning. Therefore, we introduce three regularizers into the search procedure when updating the auxiliary parameters.

**Lasso regularizer.** A naturally used sparsity regularizer is the lasso regression, which is added on the annealing-relaxed channel indicator:

$$\mathcal{R}_{\text{lasso}} = \sum_{l=1}^L \sum_{i=1}^{c_l} |H_T(\alpha_l^i)|. \quad (8)$$

$\mathcal{R}_{\text{lasso}}$  could effectively zero out some channel indicators. However, the pruning rate resulted from  $\mathcal{R}_{\text{lasso}}$  is not controllable and heavily dependent on its weight on the whole loss function.

**Continuous FLOPs estimator regularizer.** The value of the annealing-relaxed channel indicator  $H_T(\alpha_l^i)$  could be viewed as the probability of preserving the corresponding channel in the final pruned model. With the annealing-relaxed indicator of all output channels, we could estimate the expectation of overall FLOPs of the pruned model by accumulating FLOPs of each individual channel. In the  $l$ -th convolutional layer, the continuous FLOPs estimator could

be represented as:

$$E_{\text{FLOPs}}(\alpha) = \sum_{l=1}^L \left( p_l \cdot \left( \sum_{i=1}^{c_{l-1}} H_T(\alpha_l^i) \right) \cdot \left( \sum_{i=1}^{c_l} H_T(\alpha_l^i) \right) \right) \quad (9)$$

where  $p_l = h_l \times w_l \times k_l^2$ , and  $k_l$  denotes the kernel size,  $h_l$  and  $w_l$  denote the spatial size of the output feature maps.

Given the continuous FLOPs estimator, we build up the regularizer:

$$\mathcal{R}_{\text{FLOPs}}(\alpha) = \begin{cases} \log(E_{\text{FLOPs}}(\alpha)), & \frac{E_{\text{FLOPs}}(\alpha)}{F} > 1 \\ -\log(E_{\text{FLOPs}}(\alpha)), & \frac{E_{\text{FLOPs}}(\alpha)}{F} < 1 - \epsilon \\ 0, & \text{otherwise} \end{cases} \quad (10)$$

where  $F$  denotes the expected FLOPs and  $\epsilon \ll 1$ . The continuous FLOPs estimator regularizer guides DAIS to search for the optimized pruned model with FLOPs in range of  $[(1 - \epsilon) * F, F]$ .

**Symmetry regularizer.** Residual blocks are widely integrated in recent network designs, which greatly improve the capability of gradient propagation across multiple layers. The residual block is realized by adding a shortcut connection of non-parameterized identity mapping from input to output when the numbers of input and output channels are equal. However, the existing channel pruning methods (Wu et al. 2019; Dong and Yang 2019) cannot guarantee the equality between the numbers of input and output channels of a residual block, and they either drop the shortcut (Wu et al. 2019) or replace identity function with a  $1 \times 1$  convolutional layer (Dong and Yang 2019) for dimension matching. These replacements might increase the difficulty of gradient propagation across multiple layers and lead to the problem of vanishing and exploding gradients.

To verify the importance of identity mapping in the shortcut connection, we build up two network design spaces (Radosavovic et al. 2020), where multiple network instances are randomly generated with 110 layers, simulating channel pruning results of ResNet-110. All these network instances are trained 300 epochs on the CIFAR-10 dataset. Specifically, the ‘‘Random’’ design space has no constraint on the number of output channels, while in ‘‘Constrained’’ design space, every residual block is restricted to have the same

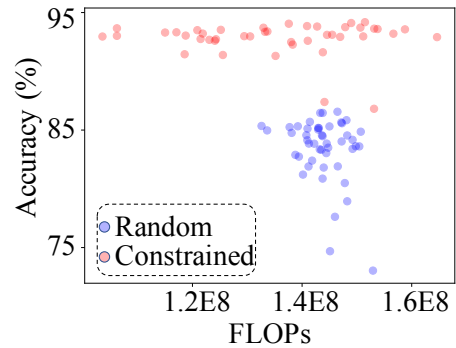


Figure 2: Statistics of 100 network instances generated from the ‘‘Random’’ and ‘‘Constrained’’ design spaces.

number of input and output channels. The generation details are described in the supplementary. With similar FLOPs  $F \in [1.1\text{E}8, 1.5\text{E}8]$ , the model instances generated from the “Constrained” design space obtain a consistent performance improvement (in terms of accuracy and pruning ratio) compared with the “Random” design space, indicating the importance of consistency between the input and output channels within a residual block.

Therefore, we propose a symmetry regularizer for channel pruning on networks with residual connections. The symmetry regularizer is defined as:

$$\mathcal{R}_{\text{sym}} = \sum_{(l, l')} \left| \left( \sum_{i=1}^{c_l} H_T(\alpha_l^i) \right) - \left( \sum_{i=1}^{c_{l'}} H_T(\alpha_{l'}^i) \right) \right|, \quad (11)$$

where  $(l, l')$  denotes a residual block with  $c_l$  input channels and  $c_{l'}$  output channels.

## 4 Experiments

### 4.1 Experiment Setup

**Datasets.** We evaluate the effectiveness of DAIS on CIFAR-10 (Krizhevsky, Hinton et al. 2009), CIFAR-100 (Krizhevsky, Hinton et al. 2009), and ImageNet ILSVRC-12 (Deng et al. 2009). CIFAR-10 and CIFAR-100 both consist of 50K training images and 10K test images, and they have 10 and 100 classes, respectively. ImageNet ILSVRC-12 contains 1280K training images and 50K test images for 1000 classes.

**Differentiable annealing indicator search.** We implement the annealing-relaxed channel indicator to each convolutional layer except for the first layer, conforming to baselines (Dong et al. 2017). The implementation details of the annealing-relaxed indicator are illustrated in the supplementary. We use  $\mathcal{R}_{\text{FLOPs}}$  and  $\mathcal{R}_{\text{sym}}$  as the default regularizers. For the update of the auxiliary parameters, DAIS adopts Adam (Kingma and Ba 2014) as the optimizer with the momentum of (0.5, 0.999), where the learning rate and weight decay rate are both set to  $1\text{E}-3$ . For the update of the network parameters, DAIS leverages the SGD optimizer with 0.9 momentum, and the learning rate is initialized with 0.1 and reduced by the cosine scheduler (Loshchilov and Hutter 2016). On the CIFAR experiments, we implement the differentiable annealing indicator search for 100 epochs. The original training images are divided into the training set and validation set with the 7 : 3 ratio. On the ImageNet experiments, we search 7508 iterations with batch size 256.

For all experiments, the auxiliary parameters are initialized with a normal distribution  $\alpha \in \mathcal{N}(1, 0.1^2)$ . The initial-ization temperature is  $T_0 = 1$ , and the temperature annealing scheme  $\sigma(n) = 49 \times n / N_{\text{max}} + 1$ , where  $N_{\text{max}}$  denotes the total number of training epochs. The batch size of the search procedure is 256. The weights of  $\mathcal{R}_{\text{FLOPs}}$  is 2 and  $\epsilon = 0.05$ . The weights of  $\mathcal{R}_{\text{sym}}$  is 0.01 for ResNet-56/110 and 0 otherwise. The weight decay of the SGD optimizer on the CIFAR and ImageNet experiments are  $5\text{E}-5$  and  $1\text{E}-5$  respectively.

**Fine-tuning.** For all experiments, we use SGD as the optimizer with a momentum of 0.9. The batch size is 256, and the learning rate is initialized with 0.1. For the CIFAR experiments, we train each model 300 epochs. The learning

rate is warmed up with 5 epochs and then reduced with the cosine scheduler. For the ImageNet experiments, we train 120 epochs for each model, and the learning rate is decayed by 10 every 30 epochs. We train all models with a single NVIDIA P40 GPU in the CIFAR experiments, and leverage 4 NVIDIA P40 GPUs in the ImageNet experiments.

### 4.2 Comparisons with State-of-the-Art Methods

**Results on CIFAR.** We first evaluate the performance of DAIS on ResNet-32/56/110 with CIFAR-10 and CIFAR-100. As illustrated in Table 1, DAIS consistently outperforms various state-of-the-art pruning approaches on CIFAR. For ResNet-32 on CIFAR-100, DAIS reduces 42.9% FLOPs and increases accuracy by 1.04% compared with the original network. Besides, DAIS only spends 95 minutes for the differentiable annealing search, while TAS finishes the search procedure in 228 minutes. For ResNet-56 on CIFAR-10, DAIS obtains greater accuracy and fewer FLOPs than GBN (You et al. 2019). Besides, since DAIS is a one-shot solution, it requires less training effort than the iterative GBN. In the case of deeper architecture ResNet-110, on both CIFAR-10 and CIFAR-100, our DAIS obtains the best FLOPs reduction ratio, accuracy drop, and accuracy, indicating that the proposed symmetry regularizer perfectly improves the capability of gradient propagation in the deeper layers.

We also evaluate the performance of DAIS on light-weighted networks like ResNet-20 and MobileNet (Howard et al. 2017). For ResNet-20 on CIFAR-10, DAIS reduces 51.1% FLOPs and increases accuracy by 0.36% compared with the original network. For MobileNet, DAIS gets better accuracy with fewer FLOPs compared with MobileNet-0.75 and CGNet (Hua et al. 2019). The experimental results are illustrated in the supplementary.

**Results on ImageNet.** To evaluate the effectiveness of DAIS, extensive experiments are performed on ResNet-18/34 (He et al. 2016) with the ImageNet dataset. We implement our model on Salaxy S9 with PyTorch Mobile<sup>1</sup>. For ResNet-18, the derived model gets  $1.68 \times$  speedup on Salaxy S9, and it exceeds the uniform pruning model by 1.44% accuracy with fewer FLOPs. For ResNet-34, the searched model by DAIS gets minimized accuracy drop and maximized pruning ratio compared with baseline methods. These experimental results verify the generality of DAIS on large scale datasets.

### 4.3 Ablation Study

**Comparison with other search methods.** To verify the effectiveness of the search procedure of DAIS, we compare the differentiable search with three other search methods. “Slimming” denotes the method (Liu et al. 2017) in which the channel indicator is represented by the weights of BN layers, and the channels with small BN weights will be filtered out. “Random” and “Constrained” are the methods mentioned in Sec. 3.4, where 50 model instances are randomly generated by each method and the instances with the best accuracy are collected in Table 3. DAIS outperforms these three methods

<sup>1</sup><https://pytorch.org/mobile/home/>

		CIFAR-10			CIFAR-100		
Depth	Method	Pruning Acc	Acc Drop	FLOPs	Pruning Acc	Acc Drop	FLOPs
32	LCCL (Dong et al. 2017)	90.74%	1.59%	4.76E7 (31.2%)	67.39%	2.69%	4.32E7 (37.5%)
	SFP (He et al. 2018a)	92.08%	0.55%	4.03E7 (41.5%)	68.37%	1.40%	4.03E7 (41.5%)
	FPGM (He et al. 2019)	92.31%	0.32%	4.03E7 (41.5%)	68.52%	1.25%	4.03E7 (41.5%)
	CNN-FCF (Li et al. 2019)	92.18%	1.07%	3.99E7 (42.2%)	-	-	-
	TAS (Dong and Yang 2019)	93.16%	0.73%	3.50E7 (49.4%)	72.41%	-1.80%	4.25E7 (38.5%)
	LFPC (He et al. 2020)	92.12%	0.51%	3.27E7 (49.4%)	-	-	-
DAIS		<b>93.49%</b>	0.57%	3.19E7 ( <b>53.9%</b> )	72.20%	-1.04%	3.94E7 ( <b>42.9%</b> )
56	LCCL (Dong et al. 2017)	92.81%	1.54%	7.81E7 (37.9%)	68.37%	2.96%	7.63E7 (39.3%)
	AMC (He et al. 2018b)	91.90%	0.90%	6.29E7 (50.0%)	-	-	-
	SFP (He et al. 2018a)	93.35%	0.56%	5.94E7 (52.6%)	68.79%	2.61%	5.94E7 (52.6%)
	FPGM (He et al. 2019)	93.49%	0.42%	5.94E7 (52.6%)	69.66%	1.75%	5.94E7 (52.6%)
	CNN-FCF (Li et al. 2019)	93.38%	-0.24%	7.20E7 (42.8%)	-	-	-
	TAS (Dong and Yang 2019)	93.69%	0.77%	5.95E7 (52.7%)	72.25%	0.93%	6.12E7 (51.3%)
	GBN (You et al. 2019)	93.07%	0.03%	3.72E7 (70.3%)	-	-	-
	GAL (Lin et al. 2019)	93.38%	0.12%	7.83E7 (37.6%)	-	-	-
	LFPC (He et al. 2020)	93.24%	0.35%	5.91E7 (52.9%)	70.83%	0.58%	6.08E7 (51.6%)
	HRank (Lin et al. 2020a)	93.17%	0.35%	6.27E7 (50.0%)	-	-	-
	ABCPruner (Lin et al. 2020b)	93.23%	0.03%	5.84E7 (54.1%)	-	-	-
	SCP (Kang and Han 2020)	93.23%	0.46%	6.10E7 (51.5%)	-	-	-
DAIS		<b>93.71%</b>	0.82%	5.61E7 (55.4%)	<b>72.57%</b>	0.81%	5.84E7 ( <b>53.6%</b> )
DAIS		93.53%	1.00%	3.64E7 ( <b>70.9%</b> )	-	-	-
110	LCCL (Dong et al. 2017)	93.44%	0.19%	1.68E8 (34.2%)	70.78%	2.01%	1.73E8 (31.3%)
	SFP (He et al. 2018a)	92.97%	0.70%	1.21E8 (52.3%)	71.28%	2.86%	1.21E8 (52.3%)
	FPGM (He et al. 2019)	93.85%	-0.17%	1.21E8 (52.3%)	72.55%	1.59%	1.21E8 (52.3%)
	CNN-FCF (Li et al. 2019)	93.67%	-0.09%	1.44E8 (43.1%)	-	-	-
	TAS (Dong and Yang 2019)	94.33%	0.64%	1.19E8 (53.0%)	73.16%	1.90%	1.20E8 (52.6%)
	GAL (Lin et al. 2019)	92.74%	0.76%	1.30E8 (48.5%)	-	-	-
	LFPC (He et al. 2020)	93.07%	0.61%	1.01E8 (60.0%)	-	-	-
	HRank (Lin et al. 2020a)	93.36%	0.87%	1.06E8 (58.2%)	-	-	-
DAIS		<b>95.02%</b>	-0.60%	1.01E8 ( <b>60.0%</b> )	<b>74.69%</b>	-0.65%	1.14E8 ( <b>56.7%</b> )

Table 1: Comparison on channel pruning approaches using ResNet on the CIFAR-10 and CIFAR-100 datasets. “Pruning Acc” = accuracy of the pruned model, “Acc Drop” = accuracy drop, “FLOPs” = FLOPs (pruning ratio). We display two pruning results of DAIS for ResNet-56 on CIFAR-10, where the first result is for best accuracy and the latter one is for best pruning rate.

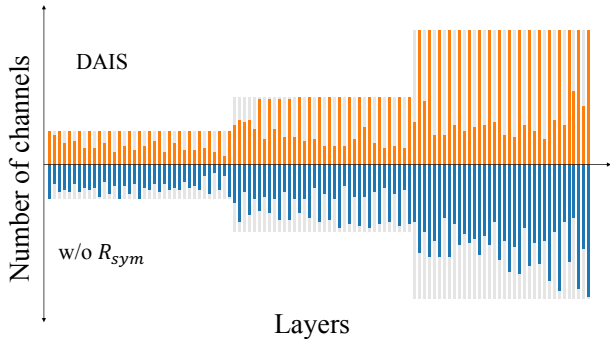


Figure 3: The pruned model for ResNet-110 on CIFAR-10.

on both the accuracy and the pruning rate, verifying the effectiveness of the differentiable annealing indicator search.

**The effectiveness of  $\mathcal{R}_{\text{FLOPs}}$  and  $\mathcal{R}_{\text{sym}}$ .** We conduct additional experiments to verify the advantages of  $\mathcal{R}_{\text{FLOPs}}$  and  $\mathcal{R}_{\text{sym}}$ . In Table 3, “w/o  $\mathcal{R}_{\text{FLOPs}}$ ” denotes a model variant that replaces  $\mathcal{R}_{\text{FLOPs}}$  by  $\mathcal{R}_{\text{lasso}}$ . The replacement leads to a huge

accuracy drop with less pruning rate, which indicates the effectiveness of  $\mathcal{R}_{\text{FLOPs}}$ . The second variant “w/o  $\mathcal{R}_{\text{sym}}$ ” removes the symmetry regularizer from DAIS and suffers a 6.05% accuracy reduction. The comparison reveals the importance of the symmetry regularizer on the ultra-deep residual networks.

Furthermore, we visualize the pruning result of DAIS and “w/o  $\mathcal{R}_{\text{sym}}$ ” in Figure 3. Compared to the pruned model derived from “w/o  $\mathcal{R}_{\text{sym}}$ ”, in each residual block, the pruned model derived from DAIS is intended to prune more channels in the first  $3 \times 3$  convolution, and reserve most channels in the second  $3 \times 3$  convolution. Therefore, the pruned model could reserve most identity functions in the shortcut path, which improves the capability of gradient propagation across multiple layers.

#### The effectiveness of the annealing-relaxed function.

With the help of the annealing-relaxed function, the channel indicator could converge to the binarization automatically without any hand-crafted thresholds. In this experiment, we explore the influences of removing the annealing-relaxed function. We design a variant “w/o annealing” which keeps the channel indicator in Eq (6) fixed without any tempera-



Depth	Method	Top-1		Top-5		FLOPs	Latency
		Prune Acc	Acc Drop	Prune Acc	Acc Drop		
18	Uniform	66.12%	3.64%	87.25%	1.83%	1.06E9 (41.8%)	0.21s (1.52 ×)
	LCCL (Dong et al. 2017)	66.33%	3.65%	86.94%	2.29%	1.19E9 (34.6%)	-
	SFP (He et al. 2018a)	67.10%	3.18%	87.78%	1.85%	1.06E9 (41.8%)	-
	ABCPruner (Lin et al. 2020b)	67.28%	2.38%	-	-	1.01E9 (44.9%)	-
	DAIS	<b>67.56%</b>	2.20%	<b>87.90%</b>	1.18%	1.03E9 (43.3%)	0.19s ( <b>1.68</b> ×)
34	PFEC (Li et al. 2017)	72.17%	1.06%	-	-	2.78E9 (24.2%)	-
	SFP (He et al. 2018a)	71.83%	2.09%	90.33%	1.29%	2.16E9 (41.1%)	-
	FPGM (He et al. 2019)	72.54%	1.38%	91.13%	0.49%	2.16E9 (41.1%)	-
	ABCPruner (Lin et al. 2020b)	70.98%	2.30%	-	-	2.17E9 (41.0%)	-
	DAIS	<b>72.77%</b>	0.54%	90.99%	0.43%	2.13E9 ( <b>41.9</b> %)	0.44s (1.36 ×)

Table 2: Comparison with baseline methods on ImageNet. “FLOPs” = FLOPs (pruning ratio). “Latency” = Latency (speedup).

	Pruning Acc	Acc Drop	FLOPs
Slimming	84.94%	9.48%	1.15E8 (54.46%)
Random	86.56%	7.86%	1.46E8 (42.15%)
Constrained	94.18%	0.24%	1.51E8 (40.17%)
DAIS	<b>95.02%</b>	-0.60%	1.01E8 ( <b>60.00</b> %)
w/o $\mathcal{R}_{\text{sym}}$	88.97%	5.45%	1.20E8 (52.62%)
w/o $\mathcal{R}_{\text{FLOPs}}$	89.15%	5.27%	1.45E8 (42.92%)
DAIS	<b>95.02%</b>	-0.60%	1.01E8 ( <b>60.00</b> %)
w/o annealing	93.57%	0.85%	1.54E8 (39.17%)
DAIS	<b>95.02%</b>	-0.60%	1.01E8 ( <b>60.00</b> %)
w/o bi-level	94.73%	-0.31%	1.04E8 (59.07%)
DAIS	<b>95.02%</b>	-0.60%	1.01E8 ( <b>60.00</b> %)

Table 3: Results of ablation study with ResNet-110 on CIFAR-10. “FLOPs” = FLOPs (pruning ratio).

ture annealing. Without temperature annealing, the  $\tilde{I}_i^t$  could not converge to the binarization automatically, and therefore we manually filter out the channels with  $\tilde{I}_i^t < 0.55$ . Results show that DAIS performs much better in terms of both accuracy and pruning ratios, verifying the necessity of the annealing-relaxed function.

**The effectiveness of the bi-level optimization.** We implement the bi-level optimization on the differentiable annealing indicator search, which updates the model parameters on the training set and updates the channel indicator on the validation set. To verify the necessity of the bi-level optimization, we design the variant “w/o bi-level” in Table 3, which jointly optimize the model parameters and channel indicators on the training set. The pruned model searched by “w/o bi-level” might overfit the training data, and results show that it performs worse on both accuracy and pruning ratio than DAIS, verifying the effectiveness of the bi-level optimization.

#### 4.4 Case Study

**Robustness of DAIS.** We first explore the impact of a shorter training scheme. The “DAIS.e50” trains 50 epochs for the differentiable annealing indicator search procedure and gets similar performance with the original DAIS, indicating the efficiency of DAIS. The second experiment explores the impact of different temperature decay schemes.

	Pruning Acc	Acc Drop	FLOPs
DAIS.e50	94.40%	0.02%	1.02E8 (59.69%)
DAIS.cosine	95.00%	-0.58%	1.04E8 (59.06%)
DAIS.smallT	94.61%	-0.19%	1.05E8 (58.70%)
DAIS	<b>95.02%</b>	-0.60%	<b>1.01E8 (60.00)</b>

Table 4: Comparisons on training schemes and temperature decay schemes with ResNet-110 on CIFAR-10. “FLOPs” = FLOPs (pruning ratio).

“DAIS.cosine” leverages a cosine decay scheme  $\sigma(n) = 49 \times (1 - \cos(\frac{\pi}{2} n / N_{\max})) + 1$ , while “DAIS.smallT” adopts a smaller termination temperature by  $\sigma(n) = 99 \times n / N_{\max} + 1$ . All variants get similar performance, which verifies the robustness of DAIS to the normal temperature decay schemes. **Recoverability.** According to (Guo, Yao, and Chen 2016), over pruning or incorrect pruning might happen in the pruning process and lead to degraded performance, and therefore the recoverability is necessary for a good pruning algorithm. Therefore, we visualize the temporary pruning results within the search procedure in the supplementary. The visualization shows that some pruned channels are recovered as the search proceeds, and the recoverability might also explain the effectiveness of DAIS.

## 5 Conclusion

In this paper, we propose Differentiable Annealing Indicator Search (DAIS), which leverages the channel indicator to represent the sparsity and searches for an appropriate pruned model with the computation cost constraints. Specifically, DAIS approximates the binarized channel indicator with the annealing-relaxed indicator and then jointly optimizes the indicator and model parameters with gradient-based bi-level optimization. The annealing-relaxed indicator will automatically converge to the binarized state as the optimization proceeds and temperature anneals. Furthermore, DAIS proposes a continuous FLOPs estimator regularizer to precisely constrain model sizes and a symmetry regularizer to optimize the gradient propagation on very deep residual networks. Experimental results show that DAIS outperforms state-of-the-art methods on CIFAR-10, CIFAR-100, and ImageNet

on different architectures, verifying the effectiveness of the differentiable search.

## Supplementary

### A Generation Details of the “Random” and “Constrained” Space

In Sec.3.4 and Sec.4.3, we introduce two network design spaces: “Random” and “Constrained”. Given an unpruned ResNet-110 model, “Random” and “Constrained” randomly generate the pruned model instances with different constraints. The generation details of “Random” and “Constrained” are as follows:

- **“Random”**. For each pruned model instance, we randomly sample the number of output channels  $c_l^{\text{Random}} = c_l * \mathcal{U}(0.5, 1)$ , where  $c_l$  denotes the number of output channels in the  $l$ -th layer of the original ResNet-110, and  $\mathcal{U}(0.5, 1)$  denotes a uniform sampling function ranging from 0.5 to 1.
- **“Constrained”**. For the model instances in the “Constrained” design space, we hope to reserve most of the identity functions in the shortcut path of the residual block, which requires the same number of input and output channels in each residual block. Therefore, we design the sampling procedure as follows. For all residual blocks in the first stage (output feature map size:  $32 \times 32$ ), we set the output channels to be  $16 * \mathcal{U}(0.5, 1)$ . For all residual blocks in the second stage (output feature map size:  $16 \times 16$ ), we set the output channels to be  $32 * \mathcal{U}(0.5, 1)$ . For all residual blocks in the third stage (output feature map size:  $8 \times 8$ ), we set the output channels to be  $64 * \mathcal{U}(0.5, 1)$ . The rest convolutional layers are randomly sampled *in the same pattern* as “Random”:  $c_l^{\text{Constrained}} = c_l * \mathcal{U}(0.5, 1)$ .

### B Implementation Details of the Annealing Channel Indicator

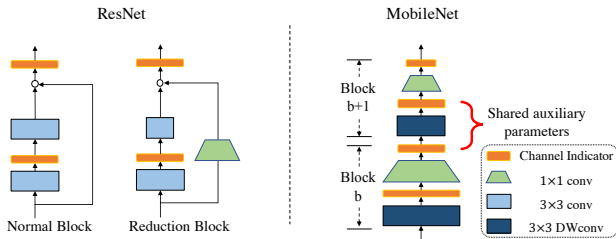


Figure 4: The channel indicator setup for ResNet and MobileNet networks.

**Implementation details on ResNet.** The original ResNet consists of two kinds of residual blocks: normal block and reduction block. Most residual blocks in the network are normal blocks, and the reduction block is employed to down-sample the spatial size of feature map while doubling the number of output channel. We adopt the same implementation for these two types of blocks: the first annealing channel indicator is used right behind the first  $3 \times 3$  convolution, and

		Pruning Acc	Acc Drop	FLOPs
R-20	LCCL (Dong et al. 2017)	91.68%	1.06%	2.61E7 (36.0%)
	SFP (He et al. 2018a)	90.83%	1.37%	2.43E7 (42.2%)
	FPGM (He et al. 2019)	91.09%	1.11%	2.43E7 (42.2%)
	CNN-FCF (Li et al. 2019)	91.13%	1.07%	2.38E7 (41.6%)
	TAS (Dong and Yang 2019)	92.88%	0.00%	2.24E7 (45.0%)
	DAIS	<b>92.89%</b>	-0.36%	1.91E7 ( <b>51.1%</b> )
M.Net	M.Net-0.75	91.65%	1.22%	1.95E8 (43.31%)
	CGNet (Hua et al. 2019)	87.56%	0.29%	1.19E8 (65.28%)
	DAIS	<b>91.87%</b>	1.00%	1.15E8 ( <b>66.60%</b> )

Table 5: Results of light-weighted networks on CIFAR-10. “R-20” and “M.Net” denote the ResNet-20 and MobileNet respectively.

	Pruning Acc	Acc Drop	FLOPs
MobileNet	92.87%	—	3.44E8
Iterative-1	91.66%	1.21%	1.88E8 (45.34%)
Iterative-2	91.76%	1.11%	1.50E8 (56.40%)
Iterative-3	91.77%	1.10%	1.18E8 (65.70%)
DAIS	<b>91.87%</b>	1.00%	1.15E8 ( <b>66.60%</b> )

Table 6: Results of iterative pruning of DAIS on CIFAR-10. “Iterative- $i$ ” denotes the  $i$ -th round pruning result by DAIS.

the second indicator is implemented after the addition of two paths. The implementation details are shown in Figure 4.

**Implementation details on MobileNet.** As shown in Figure 4, we build up the annealing-relaxed channel indicator for each  $1 \times 1$  convolution and  $3 \times 3$  depth-wise convolution (DWconv). As the DWconv requires the same number of input and output channels, the annealing-relaxed indicator is shared before and after the DWconv.

### C Extensive Experimental Results

**Results on light-weighted networks.** DAIS could achieve good performance on light-weighted networks such as ResNet-20 and MobileNet (Howard et al. 2017). On the CIFAR-10 dataset, DAIS gets better accuracy with fewer FLOPs compared with MobileNet-0.75 and CGNet (Hua et al. 2019), as shown in Table 6. The result reveals that the simple intuitive pruning rates design (evenly pruning for each layer) on MobileNet-0.75, SFP (He et al. 2018a) and FPGM (He et al. 2019) could not surpass the automatic search-based pruning approach in DAIS.

**One-shot capability of DAIS.** We conduct an iterative pruning scheme on MobileNet, denoted by “Iterative- $i$ ” in the table. Similar to most iterative pruning (Liu et al. 2020; Zhu and Gupta 2017) schemes, the pruning rate is set to be large (45%) in the first round and gradually increases 10% in latter rounds. The experimental result shows that the original one-shot DAIS obtains slightly better performance than “Iterative-3”, indicating the differentiable search procedure could effectively search the pruned models in a one-shot manner.

### D Recoverable Pruning

We visualize the differentiable annealing indicator search procedure on ResNet-20 in Table 7. For every 20 epochs,



Epochs	Number of Output Channels with $\tilde{I}_l^i > 0.5$ (from Layer 1 to Layer 19)																		
0	16	16	16	16	16	16	16	32	32	32	32	32	32	64	64	64	64	64	64
20	16	3	15	2	16	0	16	26	32	13	32	12	32	61	64	61	62	46	64
40	16	3	15	4	16	2	15	26	30	17	30	14	32	53	64	54	60	42	58
60	16	3	14	4	16	5	16	25	30	17	29	14	31	52	64	51	57	39	57
80	16	4	14	5	16	6	15	24	31	17	29	16	31	52	63	48	56	37	57
100	16	7	14	4	16	7	15	24	30	17	29	13	31	52	63	47	56	34	57

Table 7: The indicator search procedure on ResNet-20 on CIFAR-10 dataset. The number of output channels with  $\tilde{I}_l^i > 0.5$  are collected. Some channels will be firstly pruned and then recovered in the search procedure.

we collect the number of output channels with  $\tilde{I}_l^i > 0.5$ . We observe that the number of output channels does not decrease monotonically, and some channels are recovered as the training proceeds. For example, in the second convolutional layer, the number of output channels is decreased to 3, and then recovered to 7. The recoverability reveals that DAIS could rectify the mistakes of over-pruning or incorrect pruning, which might also explain the effectiveness of DAIS.

## References

2017. TensorFlow Lite. <https://www.tensorflow.org/lite>.
- Arber Zela, T. E.; Saikia, T.; Marrakchi, Y.; Brox, T.; and Hutter, F. 2019. Understanding and robustifying differentiable architecture search. *arXiv preprint arXiv:1909.09656* 2(4): 9.
- Baker, B.; Gupta, O.; Naik, N.; and Raskar, R. 2017. Designing neural network architectures using reinforcement learning. In *ICLR*.
- Bender, G.; Kindermans, P.-J.; Zoph, B.; Vasudevan, V.; and Le, Q. 2018. Understanding and Simplifying One-Shot Architecture Search. In *International Conference on Machine Learning*, 550–559.
- Chen, T.; Moreau, T.; Jiang, Z.; Zheng, L.; Yan, E.; Shen, H.; Cowan, M.; Wang, L.; Hu, Y.; Ceze, L.; et al. 2018. TVM: An automated end-to-end optimizing compiler for deep learning. In *OSDI*.
- Chen, Y.; Yang, T.; Zhang, X.; Meng, G.; Xiao, X.; and Sun, J. 2019. DetNAS: Backbone search for object detection. In *Advances in Neural Information Processing Systems*, 6638–6648.
- Chu, X.; Zhou, T.; Zhang, B.; and Li, J. 2019. Fair DARTS: Eliminating Unfair Advantages in Differentiable Architecture Search. *arXiv preprint arXiv:1911.12126*.
- Deng, J.; Dong, W.; Socher, R.; Li, L.-J.; Li, K.; and Fei-Fei, L. 2009. Imagenet: A large-scale hierarchical image database. In *Proceedings of the IEEE Conference on Computer Vision and Pattern Recognition*, 248–255. IEEE.
- Dong, X.; Huang, J.; Yang, Y.; and Yan, S. 2017. More is less: A more complicated network with less inference complexity. In *Proceedings of the IEEE Conference on Computer Vision and Pattern Recognition*, 5840–5848.
- Dong, X.; and Yang, Y. 2019. Network Pruning via Transformable Architecture Search. In *Advances in Neural Information Processing Systems*, 760–771.
- Goodfellow, I.; Pouget-Abadie, J.; Mirza, M.; Xu, B.; Warde-Farley, D.; Ozair, S.; Courville, A.; and Bengio, Y. 2014. Generative adversarial nets. In *Advances in Neural Information Processing Systems*, 2672–2680.
- Guo, Y.; Yao, A.; and Chen, Y. 2016. Dynamic network surgery for efficient dnns. In *Advances in Neural Information Processing Systems*.
- He, K.; Gkioxari, G.; Dollár, P.; and Girshick, R. 2017. Mask r-cnn. In *Proceedings of the IEEE International Conference on Computer Vision*, 2961–2969.
- He, K.; Zhang, X.; Ren, S.; and Sun, J. 2016. Deep residual learning for image recognition. In *Proceedings of the IEEE Conference on Computer Vision and Pattern Recognition*, 770–778.
- He, Y.; Ding, Y.; Liu, P.; Zhu, L.; Zhang, H.; and Yang, Y. 2020. Learning Filter Pruning Criteria for Deep Convolutional Neural Networks Acceleration. In *IEEE/CVF Conference on Computer Vision and Pattern Recognition (CVPR)*.
- He, Y.; Kang, G.; Dong, X.; Fu, Y.; and Yang, Y. 2018a. Soft filter pruning for accelerating deep convolutional neural networks. *arXiv preprint arXiv:1808.06866*.
- He, Y.; Lin, J.; Liu, Z.; Wang, H.; Li, L.-J.; and Han, S. 2018b. AMC: AutoML for Model Compression and Acceleration on Mobile Devices. In *ECCV*, 815–832. Springer.
- He, Y.; Liu, P.; Wang, Z.; Hu, Z.; and Yang, Y. 2019. Filter pruning via geometric median for deep convolutional neural networks acceleration. In *Proceedings of the IEEE Conference on Computer Vision and Pattern Recognition*, 4340–4349.
- He, Y.; Zhang, X.; and Sun, J. 2017. Channel pruning for accelerating very deep neural networks. In *Proceedings of the IEEE International Conference on Computer Vision*, 1398–1406.
- Howard, A. G.; Zhu, M.; Chen, B.; Kalenichenko, D.; Wang, W.; Weyand, T.; Andreetto, M.; and Adam, H. 2017. Mobilenets: Efficient convolutional neural networks for mobile vision applications. *arXiv preprint arXiv:1704.04861*.
- Hua, W.; Zhou, Y.; De Sa, C. M.; Zhang, Z.; and Suh, G. E. 2019. Channel gating neural networks. In *Advances in Neural Information Processing Systems*, 1884–1894.

- Jiang, X.; Wang, H.; Chen, Y.; Wu, Z.; Wang, L.; Zou, B.; Yang, Y.; Cui, Z.; Cai, Y.; Yu, T.; Lv, C.; and Wu, Z. 2020. MNN: A Universal and Efficient Inference Engine. <https://github.com/alibaba/MNN>.
- Kang, M.; and Han, B. 2020. Operation-Aware Soft Channel Pruning using Differentiable Masks. In *Proceedings of Machine Learning and Systems 2020*, 2505–2514.
- Kingma, D. P.; and Ba, J. 2014. Adam: A method for stochastic optimization. *arXiv preprint arXiv:1412.6980*.
- Krizhevsky, A.; Hinton, G.; et al. 2009. Learning multiple layers of features from tiny images.
- Li, H.; Kadav, A.; Durdanovic, I.; Samet, H.; and Graf, H. P. 2017. Pruning filters for efficient convnets. *ICLR*.
- Li, L.; and Talwalkar, A. 2019. Random search and reproducibility for neural architecture search. In *Proceedings of the Thirty-Fifth Conference on Uncertainty in Artificial Intelligence, UAI*.
- Li, T.; Wu, B.; Yang, Y.; Fan, Y.; Zhang, Y.; and Liu, W. 2019. Compressing convolutional neural networks via factorized convolutional filters. In *Proceedings of the IEEE Conference on Computer Vision and Pattern Recognition*, 3977–3986.
- Lin, M.; Ji, R.; Wang, Y.; Zhang, Y.; Zhang, B.; Tian, Y.; and Shao, L. 2020a. HRank: Filter Pruning Using High-Rank Feature Map. In *IEEE/CVF Conference on Computer Vision and Pattern Recognition (CVPR)*.
- Lin, M.; Ji, R.; Zhang, Y.; Zhang, B.; Wu, Y.; and Tian, Y. 2020b. Channel Pruning via Automatic Structure Search. In Bessiere, C., ed., *Proceedings of the Twenty-Ninth International Joint Conference on Artificial Intelligence, IJCAI 2020*, 673–679.
- Lin, S.; Ji, R.; Yan, C.; Zhang, B.; Cao, L.; Ye, Q.; Huang, F.; and Doermann, D. 2019. Towards optimal structured cnn pruning via generative adversarial learning. In *Proceedings of the IEEE Conference on Computer Vision and Pattern Recognition*, 2790–2799.
- Liu, H.; Simonyan, K.; and Yang, Y. 2019. Darts: Differentiable architecture search. In *ICLR*.
- Liu, N.; Ma, X.; Xu, Z.; Wang, Y.; Tang, J.; and Ye, J. 2020. AutoCompress: An Automatic DNN Structured Pruning Framework for Ultra-High Compression Rates. In *Proceedings of the AAAI Conference on Artificial Intelligence*, 4876–4883.
- Liu, Z.; Li, J.; Shen, Z.; Huang, G.; Yan, S.; and Zhang, C. 2017. Learning efficient convolutional networks through network slimming. In *Proceedings of the IEEE International Conference on Computer Vision*, 2736–2744.
- Liu, Z.; Sun, M.; Zhou, T.; Huang, G.; and Darrell, T. 2018. Rethinking the Value of Network Pruning. In *ICLR*.
- Loshchilov, I.; and Hutter, F. 2016. Sgdr: Stochastic gradient descent with warm restarts. *arXiv preprint arXiv:1608.03983*.
- Luo, J.-H.; Wu, J.; and Lin, W. 2017. Thinet: A filter level pruning method for deep neural network compression. In *Proceedings of the IEEE International Conference on Computer Vision*.
- Newell, A.; Yang, K.; and Deng, J. 2016. Stacked hourglass networks for human pose estimation. In *ECCV*, 483–499. Springer.
- Pham, H.; Guan, M.; Zoph, B.; Le, Q.; and Dean, J. 2018. Efficient Neural Architecture Search via Parameters Sharing. In *International Conference on Machine Learning*, 4095–4104.
- Radosavovic, I.; Kosaraju, R. P.; Girshick, R.; He, K.; and Dollár, P. 2020. Designing Network Design Spaces. *arXiv preprint arXiv:2003.13678*.
- Real, E.; Aggarwal, A.; Huang, Y.; and Le, Q. V. 2019. Regularized evolution for image classifier architecture search. In *Proceedings of the AAAI Conference on Artificial Intelligence*, volume 33, 4780–4789.
- Real, E.; Moore, S.; Selle, A.; Saxena, S.; Suematsu, Y. L.; Tan, J.; Le, Q. V.; and Kurakin, A. 2017. Large-scale evolution of image classifiers. In *International Conference on Machine Learning*, 2902–2911. JMLR. org.
- Taigman, Y.; Yang, M.; Ranzato, M.; and Wolf, L. 2014. Deepface: Closing the gap to human-level performance in face verification. In *Proceedings of the IEEE Conference on Computer Vision and Pattern Recognition*, 1701–1708.
- Tan, M.; Chen, B.; Pang, R.; Vasudevan, V.; Sandler, M.; Howard, A.; and Le, Q. V. 2019. Mnasnet: Platform-aware neural architecture search for mobile. In *Proceedings of the IEEE Conference on Computer Vision and Pattern Recognition*, 2820–2828.
- Wen, W.; Wu, C.; Wang, Y.; Chen, Y.; and Li, H. 2016. Learning structured sparsity in deep neural networks. In *Advances in Neural Information Processing Systems*.
- Wu, B.; Dai, X.; Zhang, P.; Wang, Y.; Sun, F.; Wu, Y.; Tian, Y.; Vajda, P.; Jia, Y.; and Keutzer, K. 2019. Fbnet: Hardware-aware efficient convnet design via differentiable neural architecture search. In *Proceedings of the IEEE Conference on Computer Vision and Pattern Recognition*, 10734–10742.
- Xie, S.; Zheng, H.; Liu, C.; and Lin, L. 2019. SNAS: stochastic neural architecture search. In *ICLR*.
- You, Z.; Yan, K.; Ye, J.; Ma, M.; and Wang, P. 2019. Gate decorator: Global filter pruning method for accelerating deep convolutional neural networks. In *Advances in Neural Information Processing Systems*, 2130–2141.
- Yu, R.; Li, A.; Chen, C.-F.; Lai, J.-H.; Morariu, V. I.; Han, X.; Gao, M.; Lin, C.-Y.; and Davis, L. S. 2018. Nisp: Pruning networks using neuron importance score propagation. In *Proceedings of the IEEE Conference on Computer Vision and Pattern Recognition*, 9194–9203.
- Zhu, M.; and Gupta, S. 2017. To prune, or not to prune: exploring the efficacy of pruning for model compression. *arXiv preprint arXiv:1710.01878*.
- Zhuang, Z.; Tan, M.; Zhuang, B.; Liu, J.; Guo, Y.; Wu, Q.; Huang, J.; and Zhu, J. 2018. Discrimination-aware channel pruning for deep neural networks. In *Advances in Neural Information Processing Systems*, 875–886.

Zoph, B.; and Le, Q. V. 2017. Neural architecture search with reinforcement learning. In *ICLR*.

Zoph, B.; Vasudevan, V.; Shlens, J.; and Le, Q. V. 2018. Learning transferable architectures for scalable image recognition. In *Proceedings of the IEEE Conference on Computer Vision and Pattern Recognition*, 8697–8710.